Photoionization of magnesium in the relativistic random-phase approximation

Pranawa C. Deshmukh and Steven T. Manson
Department of Physics and Astronomy, Georgia State University, Atlanta, Georgia 30303
(Received 10 March 1983)

Theoretical values for atomic photoionization cross sections, angular distribution asymmetry parameters, and spin-polarization parameters for the $3s$, $2p$, and $2s$ shells of magnesium are reported. Effects of the relativistic spin-orbit interaction and the electron-electron correlations are included by the use of the relativistic random-phase approximation in this study. Several series of autoionization resonances have been analyzed by making use of the multichannel quantum-defect theory. Comparisons with previous theoretical and experimental results where available have been made.

I. INTRODUCTION

There has recently been considerable interest in a systematic study of the photoionization processes in group-II atoms[1,2] using the relativistic random-phase approximation (RRPA).[3–5] Following the work on calcium[2] which has its ground-state configuration as $[Ar]4s^2\,{}^1S_0$, we report here our results on the study of photoionization of magnesium, which has $[Ne]3s^2\,{}^1S_0$ for its ground-state configuration. A preliminary account of this work has been presented elsewhere.[6]

Experimental data on photoabsorption by atomic magnesium are available in the vacuum ultraviolet region just above the $3s$ threshold[7] and several autoionization resonance absorption lines in the extreme ultraviolet region have been observed and characterized.[8] Photoabsorption by metallic magnesium has also been experimentally investigated.[9] Theoretical work on photoabsorption by magnesium has been concerned with the effects of electron correlations on the oscillator strengths.[10–13] The relevance of using the random-phase approximation even for light atoms such as magnesium has been already discussed.[11–13] Application of the RRPA has enabled us to investigate certain relativistic effects, for example in the asymmetry parameter for photoionization from the $3s$ subshell, as discussed below. Furthermore, in addition to studying the photoionization cross sections, angular distribution asymmetry parameters, and the spin-polarization parameters, we have made *ab initio* calculations of several autoionization resonances occurring in magnesium. The RRPA provides a natural framework to analyze the autoionization resonances since the interchannel coupling between channels open and closed for photoionization and the relativistic spin-orbit splitting are naturally built in this model. This relativistic model has enabled us to investigate the resonances occurring between the $2p_{3/2}$ and $2p_{1/2}$ thresholds also. To analyze the autoionization resonances, we have made use of the relativistic multichannel quantum-defect theory (MQDT).[14] Also, to estimate the extent to which gross features of photoionization subshell cross sections can be predicted by the Hartree-Slater (HS) central field model calculations which has been applied with fair success for several atoms,[15–18] we have performed such HS calculations on magnesium. A calculation employing an approximate HS potential is also available in the literature.[19]

We have, in fact, made use of truncated RRPA in the sense that only the correlations coming from the following nine interfering dipole channels were included:

$$3s_{1/2}\rightarrow p_{3/2},p_{1/2}\ ,$$

$$2p_{3/2}\rightarrow d_{5/2},d_{3/2},s_{1/2}\ ,$$

$$2p_{1/2}\rightarrow d_{3/2},s_{1/2}\ ,$$

and

$$2s_{1/2}\rightarrow p_{3/2},p_{1/2}\ .$$

The loss of gauge invariance resulting from the exclusion of the $1s_{1/2}\rightarrow p_{3/2}$, $p_{1/2}$ channels introduces a minor disagreement between the length and the velocity forms, which nevertheless agree within a few percent.[5]

II. PHOTOIONIZATION CROSS SECTIONS

The differential cross section for photoionization from a subshell $n\kappa$ is given by[5,20]

$$\frac{d\sigma_{n\kappa}}{d\Omega}=\frac{\sigma_{n\kappa}(\omega)}{4\pi}[1-\tfrac{1}{2}\beta_{n\kappa}(\omega)P_2(\cos\theta)]\ , \tag{1}$$

where the partial cross section $\sigma_{n\kappa}$ is given by

$$\sigma_{n\kappa}=\frac{4\pi^2\alpha\omega}{3}(\,|D_{nj\rightarrow j-1}|^2+|D_{nj\rightarrow j}|^2+|D_{nj\rightarrow j+1}|^2)\ , \tag{2}$$

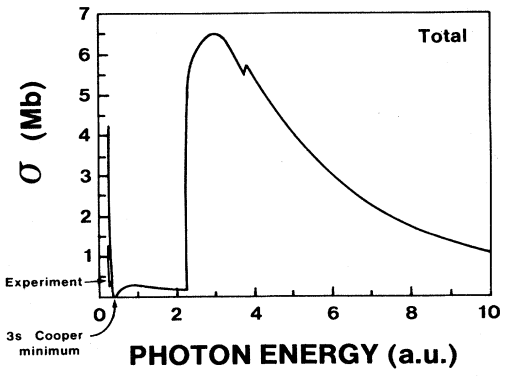

FIG. 1. Total photoionization cross section for atomic magnesium in the RRPA. The experimental curve is from Ref. 7.

$D_{nj\to j'}$ being the reduced dipole matrix element in the RRPA for the channel $nj\to j'$. In the above equations, n is the principal quantum number and the quantum number $\kappa=\mp(j+\frac{1}{2})$ for $j=l\pm\frac{1}{2}$, j and l being the one-electron total and orbital angular momentum quantum numbers. $\beta_{n\kappa}(\omega)$ in Eq. (1) is the angular distribution asymmetry parameter and ω represents the photon energy.

The total atomic photoionization cross section for magnesium is shown in Fig. 1. This figure is a composite one constructed by summing the RRPA partial cross sections for the subshells $3s$, $2p_{3/2}$, $2p_{1/2}$, and $2s$ above their respective thresholds. The thresholds for photoionization employed in the RRPA are the Dirac-Fock binding energies, which for the subshells $3s$, $2p_{3/2}$, $2p_{1/2}$, and $2s$ are, respectively, 0.2534 a.u., 2.2767 a.u., 2.2882 a.u., and 3.7801 a.u. The onset of photoionization at these thresholds enhances the total photoionization cross sections, causing sudden discontinuities at the threshold values due to opening of extra photoionization channels, as can be seen in Fig. 1. The experimental cross section measured by Ditchburn and Marr[7] is also shown in the same figure. Both the theory and experiment show a rapid drop in the cross section just above the $3s$ threshold toward the "Cooper" minimum[21–23] (also called "Ditchburn-Bates-Seaton-Cooper" minimum[24]) for the $3s$ subshell, which in the RRPA occurs at a photon energy of $\sim$0.408 a.u. The RRPA value at the $3s$ threshold is larger than the experimental value due to neglect of multiconfigurational interactions in the RRPA, which lead to certain two-electron correlations.[2] Other features in Fig. 1 can be understood in terms of the partial cross sections of the various subshell photoionization which are discussed below. It should be noted that in the region of the autoionization resonances, Fig. 1 shows only the background cross section, and the departures from the background value due to autoionization resonances are discussed later using the MQDT.

The RRPA partial cross section for the $3s$ subshell is shown in Fig. 2 along with the corresponding result in the Hartree-Slater approximation. The present RRPA results for the $3s$ cross section are in complete agreement with the nonrelativistic random-phase approximation exchange (RPAE) calculations of Amusia *et al.*[12] and also with the HS results with regard the overall profile of the energy dependence of the cross section. This is not surprising since relativistic effects on $3s$ cross section in magnesium are not significant. The angular distribution asymmetry parameter for photoionization from the $3s$ subshell does, however, show a difference between the RRPA and the RPAE schemes, at the Cooper minimum, as will be seen later. The Cooper minimum in $3s$ photoionization is seen in Fig. 2, as in Fig. 1. Over the entire range of energy studied, the RRPA and HS results of Fig. 2 are in good agreement, except that the RRPA curve shows a mild shoulder above the HS curve in the neighborhood of 2.3 a.u., just above the $2p_{3/2}$, $2p_{1/2}$ thresholds, resulting from interchannel coupling.

Figure 3 is a composite of partial photoionization cross sections from the $2p_{3/2}$ and the $2p_{1/2}$ thresholds which occur at 2.2767 and 2.2882 a.u., respectively. The portion of the RRPA curve above the $2p_{1/2}$ threshold is made up from the sum of the two individual cross sections for the $2p_{3/2}$ and $2p_{1/2}$ subshells, and in the narrow gap between

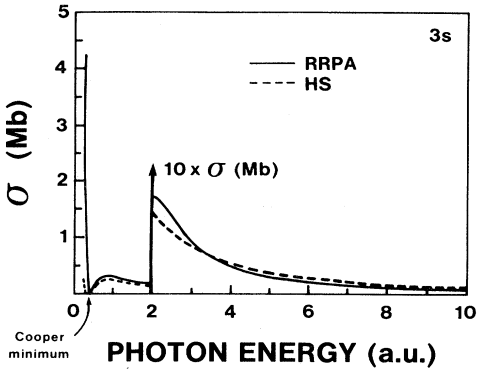

FIG. 2. Partial cross section for the $3s$ shell.

these two thresholds only the background cross section for photoionization from the $2p_{3/2}$ subshell is shown; the autoionization resonances being considered separately later. The HS cross section is also shown in the same figure. Remembering the fact that the HS and RRPA thresholds are not at the same energy, one can see a good agreement between these two model calculations. The RPAE calculations of Amusia *et al.*[12] are also in very good agreement with the present RRPA results. The remarkable agreement between the RRPA, RPAE, and HS calculations suggests that in the consideration of the gross features of the partial cross section for photoionization from the $2p$ shell of magnesium, neither relativity for interchannel coupling plays a very major role.

It is interesting to compare the partial photoionization cross section for the $2p$ shell of magnesium with that for the $3p$ shell of calcium,[2] which is right below magnesium in the periodic table. These two atoms have similar ground-state configurations. However, while the $3p$ orbital in calcium has one node and shows a Cooper minimum, the $2p$ orbital in magnesium being nodeless does not have a Cooper minimum. Thus, unlike calcium, in which the $3p$ photoionization cross-section goes through a Cooper minimum, the $2p$ cross section in mag-

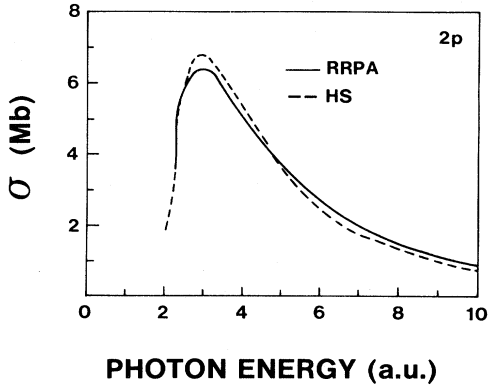

FIG. 3. Partial cross section for the $2p$ shell. The portion above the $2p_{1/2}$ threshold is the sum of the partial cross sections for photoionization from the $2p_{3/2}$ and $2p_{1/2}$ subshells.

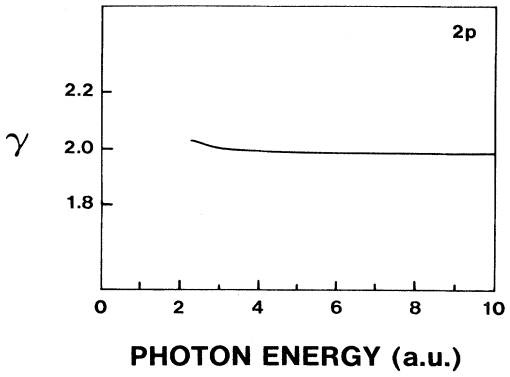

FIG. 4. Branching ratio for the $2p$ shell.

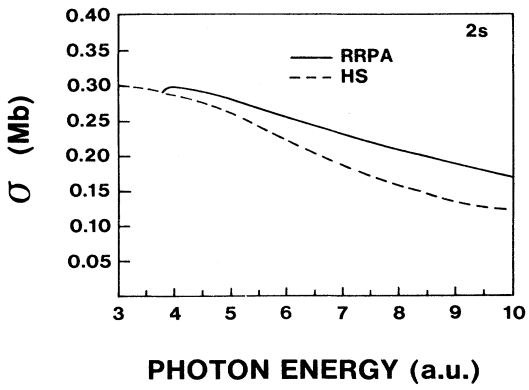

FIG. 5. Partial cross section for the $2s$ shell.

nesium actually first rises above the threshold value. The difference between the Ca $3p$ and Mg $2p$ case comes from, besides the number of nodes in the p-orbital, the nature of the one-electron centrifugal barrier potential.[23] In calcium, the $3d$ state is just about to get bound,[2,25] so the centrifugal carrier to $p \rightarrow d$ type dipole ionization channels has minimal effect. For magnesium, however, the centrifugal barrier does cause a "delayed onset" in the transition probability showing as a "shape resonance,"[26] as can be seen in Fig. 3. This same "hump" shows up in Fig. 1 also as most of the contribution to the total photoionization cross section in the corresponding energy region comes from the ionization of the $2p$ shell.

The absence of Cooper minimum in magnesium $2p$ photoionization as against the Ca $3p$ case,[2] as also the different nature of the centrifugal barrier to photoionization in these two cases, manifests in a somewhat different energy dependence for magnesium of the branching ratio, which is given by

$$\gamma = \sigma_{p_{3/2}} / \sigma_{p_{1/2}} . \tag{3}$$

The statistical value for γ is 2. However, for calcium[2] the $3p_{3/2}$ cross section goes through its Cooper minimum at a slightly lower energy than that at which the $3p_{1/2}$ cross section does, causing interesting deviation from the statistical value of γ in the neighborhood of the Cooper minima. In the case of magnesium, by contrast, there being no Cooper minimum in the $2p$ cross sections, the branching ratio stays basically close to the statistical value, as is shown in Fig. 4. However, as can be seen in this figure, the branching ratio is very slightly greater than 2 just above the $2p_{1/2}$ threshold. The curve in Fig. 4 is plotted for energies greater than the $2p_{1/2}$ binding energy. Now, at the energy at which the $2p_{1/2}$ ionization channels open up, photoionization from the $2p_{3/2}$ subshell has already overcome the centrifugal barrier effect to some extent causing γ to be slightly greater than 2 at the $2p_{1/2}$ threshold. Such a detailed behavior of γ will of course not emerge from a nonrelativistic calculation.

The partial cross section for photoionization from the $2s$ shell is shown in Fig. 5 in both the RRPA and the HS approximation. The $2s$ thresholds in the two models are not at the same energy, but considering this difference there is an overall fair agreement between the $2s$ cross sections predicted by the two methods. Nevertheless, the RRPA cross section shows a minor shape resonance caused by a relatively mild centrifugal barrier which the final-state p wave functions face in the construction of the transition matrix element. Furthermore, interchannel coupling, mainly with photoionization channels from the $2p$ subshells, in the RRPA causes the $2s$ cross section to be driven above that in the HS model, since in the entire energy range shown in Fig. 5, photoionization from the $2p$ subshells is the dominant factor. Among the $3s$, $2p$, and $2s$ photoionization cross sections studied here, it is only the $2s$ cross section which shows some difference when calculated in the RRPA rather than the HS approximation. It is only in this case that the interchannel coupling becomes a significant factor. To appreciate this feature, it may be noted that in the energy range above the $2s$ threshold, the $2p$ cross section is roughly 10 times larger than the $2s$ cross section. As a result of this, the interchannel coupling between ionization channels from the $2p$ and $2s$ shells affects the $2s$ cross section far more than the $2p$ cross section. Thus the agreement between the HS and RRPA results is much better for $2p$ than the $2s$ cross section.

III. ANGULAR DISTRIBUTION OF THE PHOTOELECTRONS

The study of the angular distribution of photoelectrons relative to the incident-photon direction is a very powerful tool in extracting and separating geometrical and dynamical factors involved in the photoionization process.[27–31] In particular, the energy dependence of the angular distribution asymmetry parameter β gives vital information about effects due to interchannel coupling, the relativistic interactions, and also about the suitability of any chosen angular momentum coupling scheme for the species which is the seat of photoionization.[31] In the present study, therefore, we have investigated the energy dependence of β for photoionization from the $3s$, $2p$, and $2s$ shells of magnesium.

Magnesium, being a low-Z atom, is satisfactorily expressed in the LS coupling scheme and since it is a closed-shell atom, the nonrelativistic value for β for photoionization from its s shells is essentially 2, independent of ener-

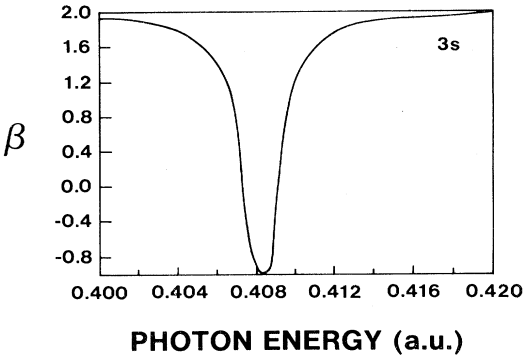

FIG. 6. Angular distribution asymmetry parameter for photoionization from the $3s$ shell near its Cooper minimum.

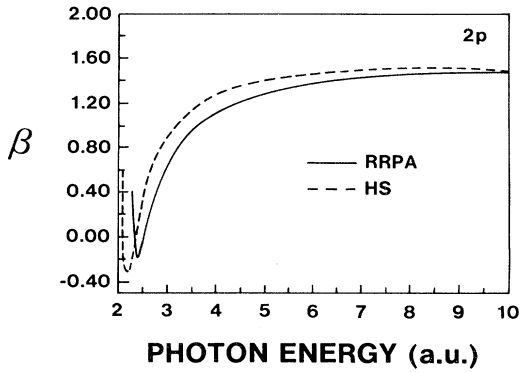

FIG. 7. Angular distribution asymmetry parameter for photoionization from the $2p$ shell.

gy.[27–31] This corresponds to a pure $\cos^2\theta$ dependence of the photoionization yield, where θ is the angle between the electric field vector of the incident photon and the direction of photoejection with regard to photoionization from an unpolarized target due to incident linearly polarized light. This nonrelativistic picture envisages a single $s \rightarrow p$ photoionization channel. However, the relativistic electron-ion interaction permits an extra channel for photoionization resulting in an energy-dependent departure from the nonrelativistic value 2, depending on the relative strengths in the two channels. These effects are most striking near cross-section minima where the relative amplitude in the two channels varies rapidly with energy. These details have been analyzed at length in a recent review[31] for photoionization from the s shell of both closed- and open-shell atoms.

The relativistic expression for β for photoionization from the s shell of a closed-shell atom given as a function of the photon-energy is[5]

$$\beta_s(\omega)=2-\frac{3\,|A_T(\omega)|^2}{|A_S(\omega)|^2+|A_T(\omega)|^2}\,, \tag{4}$$

wherein $A_T(\omega)$ and $A_S(\omega)$ are the dipole transition amplitudes into, respectively, triplet and singlet states. The departure from the nonrelativistic value of 2 for β_s becomes most dramatic near the Cooper minimum. The asymmetry parameter β_{3s} for photoionization from the $3s$ shell of magnesium is shown in Fig. 6 in the energy region near the Cooper minimum for that shell, which occurs at $\sim$0.408 a.u. (Fig. 2). It may be noted that at this energy the $3s$ cross section is not exactly equal to zero because the $3s \rightarrow p_{1/2}$ and $3s \rightarrow p_{3/2}$ channels do not go through their respective Cooper minima exactly at the same energy. Nevertheless, at $\sim$0.408 a.u., the singlet amplitude very nearly vanishes and hence, according to Eq. (4), $\beta_{3s}(\omega)$ at this energy becomes nearly equal to -1, giving a photoelectric yield perpendicular to the electric vector of the incident photon. This feature is seen to be borne out in Fig. 6.

The overall profile for β_{3s} near the $3s$ Cooper minimum for magnesium is very similar to that for sodium,[31] its lower neighbor in the periodic table. Moreover, the width in the variation of β, which has been shown to increase with atomic number,[31] is also about the same in sodium and magnesium, since the atomic number of magnesium exceeds that of sodium just by one.

The asymmetry parameter for photoionization from the $2s$ shell of magnesium has been found to be nearly equal to 2, the nonrelativistic value, for the entire range of photon energies considered in the present RRPA calculations, since only the photoionization channel into the singlet state predominates, leading to a single-channel energy-independent β.[31]

While considering the angular distribution asymmetry parameter for photoionization from the $2p$ shell of magnesium, we recognize the fact that even for the nonrelativistic point of view, two photoionization channels exist for closed-shell atoms corresponding to $p \rightarrow s$ and $p \rightarrow d$ dipole transitions. Thus even a nonrelativistic estimate of β would show an energy dependence determined by the relative strengths in these two channels. The interference between these two channels changes with energy as the phase shifts and the relative amplitudes are both energy dependent.[30] The asymmetry parameter β_p for photoionization from the p shells for a large number of atoms over a wide range of energies has been investigated in the nonrelativistic HS approximation[30] and a rapid variation of β_p in the threshold region has been observed. It has been found to be strongly dependent on the existence, or otherwise, of a Cooper minimum in the $p \rightarrow d$ channel. Relativistically, the np level breaks down into $np_{1/2}$ and $np_{3/2}$ levels due to the spin-orbit interaction. Thus the ion after photoejection can be left into $2p_{1/2}$ or $2p_{3/2}$ states corresponding to which a totality of five relativistic photoionization channels exist, as indicated in Sec. I above. In the present calculations, therefore, $\beta_{2p_{3/2}}$ and $\beta_{2p_{1/2}}$ were calculated in the RRPA and β_{2p} was calculated in the nonrelativistic HS approximation. The results are shown in Fig. 7 in which the RRPA curve has been plotted using the following weighted average:

$$\beta_{2p}^{\mathrm{RRPA}}(\omega)=\frac{\sigma_{2p_{3/2}}(\omega)\beta_{2p_{3/2}}(\omega)+\sigma_{2p_{1/2}}(\omega)\beta_{2p_{1/2}}(\omega)}{\sigma_{2p_{3/2}}(\omega)+\sigma_{2p_{1/2}}(\omega)}\,. \tag{5}$$

The rapid variation in β_{2p} in the near-threshold region

involving a drop in the value of β above the threshold to a minimum and its eventual rise is strongly influenced by the fact that $p \rightarrow s$ and $p \rightarrow d$ channels show strong energy-dependent interference. Since the $2p$ cross section has no Cooper minimum, no major discrepancy between the relativistic and the nonrelativistic calculations is expected, and accordingly the present RRPA and the HS results are in very good agreement, as can be seen in Fig. 7.

IV. SPIN POLARIZATION OF THE PHOTOELECTRONS

It is well known that a nonrelativistic theory predicts no spin polarization of the photoelectrons ejected from both the s- or the p-type shells.[32,33] A relativistic theory does, however, account for the net spin polarization.[34,35] Using the notations of Huang,[34] the x, y, and z components of the spin-polarization vector P are given in terms of dynamical spin-polarization parameters (ξ,η,ζ,δ) which can be written in terms of the weighted sums of the dipole matrix elements. The RRPA matrix elements can be employed toward this. For the case of incident circularly polarized radiation, one has the following relations[34,35]:

$$P_x = \pm\xi \sin\theta / F(\theta) , \tag{6a}$$

$$P_y = \eta \sin\theta \cos\theta / F(\theta) , \tag{6b}$$

$$P_z = \pm\zeta \cos\theta / F(\theta) , \tag{6c}$$

and

$$P_{\text{tot}} = \pm\delta , \tag{6d}$$

where

$$F(\theta) = 1 - \tfrac{1}{2}\beta P_2(\cos\theta) \tag{7a}$$

and

$$\delta = (\zeta - 2\xi)/3 . \tag{7b}$$

In the above equations, it is assumed that the z axis is along the direction $\vec{p}$ of the outgoing electron, the y axis along $\vec{k}\times\vec{p}$, and the x axis along $[\vec{k}\times\vec{p}]\times\vec{p}$, $\vec{k}$ being the direction of the incident photon. The $\pm$ sign in the above equations refers to the helicity of the incident photon being positive or negative.

For magnesium, as in the case of calcium,[2] the $3s$ and $2s$ spin-polarization parameters are nearly zero. The parameters for the $2p_{3/2}$ subshell of magnesium are shown in Fig. 8. The spin-polarization parameters for the $2p_{1/2}$ subshell are approximately double in magnitude and opposite in sign relative to those of the $2p_{3/2}$ subshell, so when weighted by their respective photoionization cross sections, the net spin polarization approximately cancels out approaching the nonrelativistic limit.

V. AUTOIONIZATION RESONANCES

The analysis of the autoionization resonances is a matter of prime concern in the interpretation of the arc spectra of the alkaline-earth elements.[8] The RRPA provides a natural framework to analyze the autoionization resonances from a theoretical viewpoint since the interference between channels open and closed for photoionization is automatically built in it. However, for practical considerations, it is very convenient to supplement the RRPA analysis with the relativistic MQDT.[14,36–39] The extraction of the MQDT dynamical parameters in an *ab initio* manner from the RRPA makes it possible[14,39] to obtain detailed information about the autoionization resonances, which have not been considered in the nonrelativistic RPA calculations.[12,13] Three different sets of resonances have been analyzed in the present work.

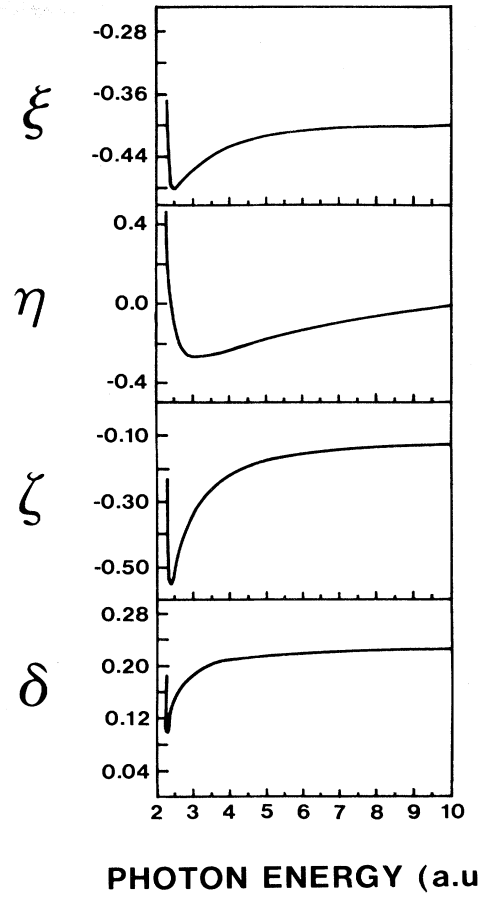

FIG. 8. Spin-polarization parameters for the $2p_{3/2}$ subshell.

A. Autoionization resonances in the $2p_{3/2}$ and $2p_{1/2}$ cross sections below the $2s$ threshold

At incident-photon energies slightly below the binding energy for the $2s$ level, there is substantial interference between photoexcitation channels from $2s$ to discrete $p_{1/2}$ and $p_{3/2}$ states and the photoionization channels originating in the $2p_{3/2}$ and $2p_{1/2}$ levels leading to autoionizing resonances. Depending on the nature of this interference being constructive or destructive, the net cross section at the resonance energies for photoionization from the $2p_{3/2}$ and $2p_{1/2}$ subshells rises or decreases, respectively, about the background value.

Photoionization channels from the $3s$ shell have a very small cross section in this region and are thus excluded. Accordingly, we have made this analysis using the follow-

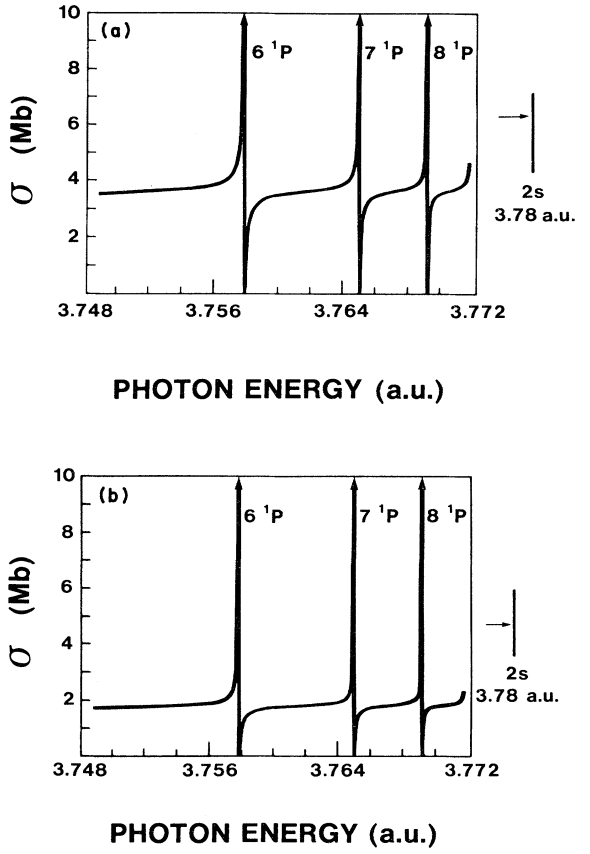

FIG. 9. (a) Autoionization resonances in the $2p_{3/2}$ cross section converging to the $2s$ threshold. The final states in the discrete excitations of the $2s$ electrons involved in the autoionization processes are indicated. (b) Autoionization resonances in the $2p_{1/2}$ cross section converging to the $2s$ threshold. The final states in the discrete excitations of the $2s$ electrons involved in the autoionization processes are indicated.

ing seven channels:

$$2s \rightarrow p_{1/2},p_{3/2} \text{ (discrete excitations)},$$

$$2p_{1/2} \rightarrow s_{1/2},d_{3/2} \text{ (ionization into continuum)},$$

and

$$2p_{3/2} \rightarrow s_{1/2},d_{3/2},d_{5/2} \text{ (ionization into continuum)}.$$

Of the two sets of autoionization resonances corresponding to discrete excitations from the $2s$ shell into singlet and triplet states, only those to the singlets are significant. These lead to autoionization resonances in the $2p_{3/2}$ and $2p_{1/2}$ photoionization cross sections which are shown, respectively, in Figs. 9(a) and 9(b). The resonances shown in these figures correspond to a quantum defect $\mu=1.31$. The principal quantum number n in the $2s_{1/2} \rightarrow np_{1/2}$ discrete transitions is also indicated in the same figures. It may be noted from these figures that the background cross sections for the $2p_{3/2}$ and $2p_{1/2}$ resonances are, respectively, about 3.6 and 1.8 Mb in the statistical ratio 2:1. Moreover, their sum (5.4 Mb) approximately corresponds to the $2p$ photoionization cross section shown in Fig. 3, near the neighborhood of the $2s$ threshold. Both constructive and destructive effects of the interference are visible, and one can see that these resonances converge to the $2s_{1/2}$ threshold occurring at 3.78 a.u.

B. Autoionization resonance in the $3s$ and the $2p_{3/2}$ cross sections between the $2p_{3/2}$ and $2p_{1/2}$ thresholds

At incident photon energies between the $2p_{3/2}$ and $2p_{1/2}$ thresholds, the $2p_{1/2} \rightarrow s_{1/2},d_{3/2}$ discrete excitations interfere with photoionization channels originating in the $3s_{1/2}$ and $2p_{3/2}$ levels leading to autoionization resonances. Accordingly, the following seven interacting channels are involved in the resonance process:

$$3s_{1/2} \rightarrow p_{1/2},p_{3/2} \text{ (ionization into continuum)},$$

$$2p_{3/2} \rightarrow s_{1/2},d_{3/2},d_{5/2} \text{ (ionization into continuum)},$$

and

$$2p_{1/2} \rightarrow s_{1/2},d_{3/2} \text{ (discrete excitations)}.$$

We have made the MQDT analysis of these resonances using the above seven channels. The discrete transitions $2p_{1/2} \rightarrow ns_{1/2}$ or $nd_{3/2}$ lead to autoionizing resonances in the $3s_{1/2}$ and $2p_{3/2}$ photoionization cross sections which are shown, respectively, in Figs. 10(a) and 10(b). The principal quantum numbers n of the Rydberg-series discrete states are also indicated in the same figures. One can see that both the sets of resonances are converging to the $2p_{1/2}$ threshold, occurring at ~ 2.288 a.u.

Some absorption lines in the discrete Rydberg excitation spectrum of magnesium have been observed and characterized by Newsom.[8] It is interesting to compare the quantum defects obtained in the present RRPA + MQDT study and those given by Newsom.

Newsom has characterized $2p_{1/2} \rightarrow ns_{1/2}$ discrete transitions and has assigned for the quantum defects of the discrete final states for $n=4$ through $n=9$ values between 1.78 and 2.00. The present analysis gives for the quantum defects for the $2p_{1/2} \rightarrow ns_{1/2}$ resonances, shown in Figs. 10(a) and 10(b), a value of 1.81, in good agreement with Newsom's assignment.

The RRPA + MQDT quantum defect for the $d_{3/2}$ states involved in the discrete Rydberg-series $2p_{1/2} \rightarrow nd_{3/2}$ transitions leading to the other set of resonances shown in Figs. 10(a) and 10(b) is 0.28. This is somewhat lower than the range (0.38—0.72) of quantum defects assigned by Newsom corresponding to the principal quantum number n having values 3 through 9. This discrepancy can be understood by recognizing the fact that for the lowest members of the Rydberg series, the quantum defects vary rather rapidly. For example, Newsom's assignment of $\mu=0.72$ for $n=5$ is almost the double of $\mu=0.38$ for $n=3$. The quantum defect 0.28 obtained in the present analysis corresponds to higher members ($n>8$) of the Rydberg series. In this respect, it is important to note that whereas in an experiment it is easier to

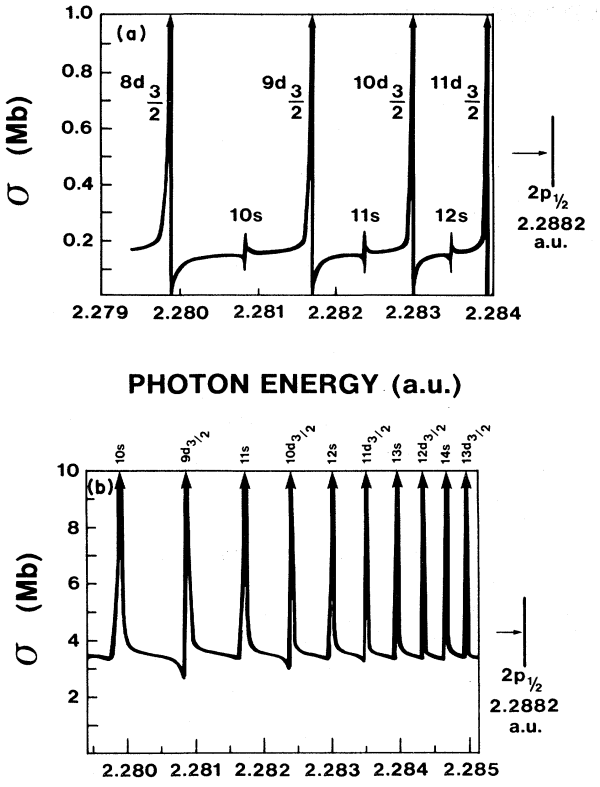

FIG. 10. (a) Autoionization resonances in the $3s$ cross section between the $2p_{3/2}$ and $2p_{1/2}$ thresholds. The final states in the discrete excitations of the $2p_{1/2}$ electrons involved in the autoionization processes are indicated. (b) Autoionization resonances in the $2p_{3/2}$ cross section converging to the $2p_{1/2}$ threshold. The final states in the discrete excitations of the $2p_{1/2}$ electrons involved in the autoionization processes are indicated.

analyze the lower members of the Rydberg series than the higher ones, due to the increase in the demand on experimental resolution for the higher members, the situation in our theoretical analysis is just the opposite. The RRPA + MQDT analysis[14] of the autoionization resonances rests on the quantum defects being only weakly energy dependent, making the analysis easier for higher members of the Rydberg series. The experiment and the theory thus face difficulties in different regions of the Rydberg series and thereby are of complementary value. The agreement between theory ($\mu=1.81$) and experiment ($\mu=1.78$ to 2.00) for the quantum defects for the discrete $ns_{1/2}$ states is of course good, as mentioned before, but in this case the percentage change in the quantum defects across the Rydberg series is indeed small, as can be seen from Newsom's assignments.[8]

C. Autoionization resonances in the 3s cross section below the $2p_{3/2}$ threshold

Just below the ionization threshold for the $2p_{3/2}$ level, resonances occur in photoionization from the $3s$ shell due

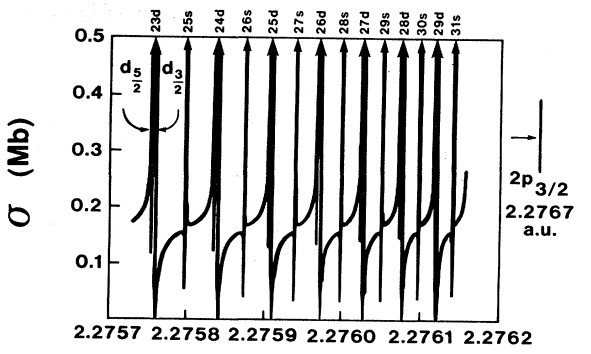

FIG. 11. Autoionization resonances in the $3s$ cross section below the $2p_{3/2}$ threshold. The final states indicated are those of the discrete excitations of the $2p_{3/2}$ electrons involved in the autoionization processes.

to interference with discrete transitions of the electrons in the $2p_{3/2}$ level. Moreover, even the Rydberg series converging to the $2p_{1/2}$ threshold have some members below the $2p_{3/2}$ threshold, leading to the autoionization resonances in the $3s$ photoionization. The following seven channels were therefore included in the RRPA + MQDT analysis of these resonances:

$$3s_{1/2}\rightarrow p_{1/2},p_{3/2} \text{ (ionization into continuum)},$$

$$2p_{3/2}\rightarrow s_{1/2},d_{3/2},d_{5/2} \text{ (discrete excitations)},$$

$$2p_{1/2}\rightarrow s_{1/2},d_{3/2} \text{ (discrete excitations)}.$$

In particular, $2p_{1/2}\rightarrow ns_{1/2}$ for $n=4$–8 and $2p_{1/2}\rightarrow nd_{3/2}$ for $n=3$–6 lead to autoionization resonances in the $3s$ cross section below the $2p_{3/2}$ threshold. Higher members of the Rydberg series in these two sets of discrete transitions lie in between the $2p_{3/2}$ and $2p_{1/2}$ thresholds. The corresponding autoionization resonances extracted from the RRPA + MQDT analysis are shown in Fig. 11. Of the five interfering Rydberg series, three converge to the $2p_{3/2}$ threshold ($2p_{3/2}\rightarrow s_{1/2},d_{3/2},d_{5/2}$). In Fig. 11, these are shown for somewhat high members of the Rydberg series. The principal quantum numbers of the final states in the discrete transitions are also indicated in Fig. 11, in which the resonances are seen to converge on the $2p_{3/2}$ threshold which occurs at 2.2767 a.u. Lower members of the Rydberg series have not been analyzed due to rapid variations in the MQDT parameters, as explained before. Of the remaining two Rydberg series, the members $2p_{1/2}\rightarrow nd_{3/2}$ for $n=3$, 4, 5, and 6 and $2p_{1/2}\rightarrow ns_{1/2}$ for $n=4$, 5, 6, 7, and 8 occur at photon energies lower than those considered in Fig. 11. The higher members occur at energies above the $2p_{3/2}$ threshold. Thus, in Fig. 11, only three out of the five interfering Rydberg series below the $2p_{3/2}$ threshold are seen to manifest as autoionization resonances in the $3s_{1/2}$ cross section. The quantum defects for the final states in the discrete $2p_{3/2}\rightarrow s_{1/2}$, $d_{3/2}$, and $d_{5/2}$ resonances shown in Fig. 11 are, respectively, 1.78, 0.28, and 0.34. The quantum defect for the final states of the s type agrees very well with

Newsom's assignments.[8] Newsom has assigned to the quantum defects for the $4s_{1/2}, 5s_{1/2}$, and $6s_{1/2}$ levels the values 1.77, 1.72, and 1.77, respectively. These seem to be pretty much stable even for higher members of the Rydberg series as the present analysis shows. Newsom's assignment of quantum defects for $nd_{3/2}$ final states are lower than those for the $nd_{5/2}$ final states, as one would expect, and as is in agreement with present RRPA + MQDT analysis. However, the experimentally obtained quantum defects for the lower members of the $2p_{3/2} \rightarrow nd_{3/2}$ and $nd_{5/2}$ series show substantial variation and the apparent discrepancy with the theoretical estimate should be understood in the context of the remarks made in the previous case.

In examining the discrepancy between the quantum defects determined experimentally and theoretically for the $nd_{3/2}$ and $nd_{5/2}$ final states involved in the autoionization resonances discussed above, the following difficulties in (i) the experimental assignments of the spectral lines and (ii) theoretical calculation of the quantum defects should be remembered.

The assignments of spectral lines as belonging to a particular Rydberg series observed in an experiment depends on the accurate determination of the series limits. In the cases discussed above we have three Rydberg series converging to the $2p_{3/2}$ and two to the $2p_{1/2}$ threshold. The unscrambling of the spectral assignments could be in serious error if the limits are not determiend very accurately, and the quantum defects evaluated from them would consequently be erroneous.

The present theoretically determined quantum defects could be in error in as much as they are determined by the RPA methodology which includes only some of the correlations.[40] For example, ground-state configuration mixing $3s^2\,{}^1S_0$ with $nln'l'\,{}^1S_0$ states are excluded as also the final-state mixing of $3s\epsilon p$: $(J=1)$ with $3pns$ and $3pnd$ $(J=1)$ states. Despite these limitations of the RPA method, we believe that the theoretical findings of the present work are probably fairly reliable. A review of the experimental assignments of the autoionization resonances will help clarify the discrepancies between the theoretical and experimental quantum defects where they appear. Very close to the first threshold, however, the ${}^1S_0$ configurations involving virtual excitations to different spin orbitals may cause significant correlations, the neglect of which may cause inaccuracies in predicting, for example, the cross section at the first threshold.

Finally, we wish to point out the importance of providing for a departure from the *LS* coupling scheme even for magnesium (which has such a low atomic number), while analyzing its autoionization resonances. The suitability of the *LS* or the *jj* designation depends on the ratio of electrostatic to magnetic interactions[41] which changes in favor[42] of the *jj* coupling scheme for higher members of a Rydberg series, making its provision important.

IV. CONCLUSIONS

The overall agreement between results of the RRPA and the HS calculations of the gross features of the photoionization process is the result of the fact that both relativistic effects and the interchannel coupling play a fairly minor role in the photoionization process for magnesium, it being a rather low Z atom. Nevertheless, relativistic effects result in a dramatic departure of the angular distribution asymmetry parameter β for photoionization from the $3s$ shell near its Cooper minimum, and interchannel coupling significantly affects the cross section for photoionization from the $2s$ shell. Since the $2p$ shell has no Cooper minimum, there is no significant discrepancy between the RRPA and the HS results even for the angular distribution asymmetry parameter. The HS results are presented in this study not to suggest that the HS model competes with the RRPA (which is clearly far superior), but only to demonstrate to what extent a simple calculation can bring out at least the gross features in the photoionization process.

Several series of autoionization resonances accompanying the principal photoionization process in magnesium have been analyzed in this work by supplementing the RRPA results by making use of the MQDT. Comparison between the quantum defects for the discrete final states involved in the autoionization process as obtained in the present theoretical analysis and as obtained from experimental characterizations, where available, leads to good agreement for the $ns_{1/2}$ discrete final states, and not so good agreement for the $nd_{3/2}$ and the $nd_{5/2}$ discrete final states. While attempting such comparisons, it is pointed out that the experiment and the theory face difficulties in the higher and the lower members, respectively, of any given Rydberg series, thus being of complementary value. The suitability of different angular momentum coupling schemes in the analysis of the autoionization resonances in different regions of a Rydberg series has been pointed out. A review of the experimental assignments[8] of the five interacting Rydberg series in the neighborhood of the $2p_{1/2}, 2p_{3/2}$ thresholds is urged.

ACKNOWLEDGMENTS

The Dirac-Fock functions for magnesium were generated using the computer code of Professor W. R. Johnson. The RRPA and the MQDT analysis has been done using the codes originally written by Professor W. R. Johnson and updated by Professor W. R. Johnson and Dr. K. T. Cheng. The spin-polarization analysis is based on the work of Dr. K.-N. Huang. We are grateful to Professor W. R. Johnson for supplying us the computer codes and for his help and constructive comments at all stages of this work. Helpful discussions with Dr. K. T. Cheng, Dr. V. Radojević, and Dr. K.-N. Huang are also gratefully acknowledged. This work was supported by the U. S. Army Research Office.

[1]W. R. Johnson, V. Radojević, P. Deshmukh, and K. T. Cheng, Phys. Rev. A 25, 337 (1982).

[2]P. C. Deshmukh and W. R. Johnson, Phys. Rev. A 27, 326 (1983).

[3]W. R. Johnson, C. D. Lin, and A. Dalgarno, J. Phys. B 9, L303 (1976).

[4]W. R. Johnson and C. D. Lin, Phys. Rev. A 20, 964 (1979).

[5]W. R. Johnson, C. D. Lin, K. T. Cheng, and C. M. Lee, Phys. Scr. 21, 409 (1980).

[6]P. C. Deshmukh and S. T. Manson, Bull. Am. Phys. Soc. 27,

472 (1982).
[7]R. W. Ditchburn and G. B. Marr, Proc. Phys. Soc. A66, 655 (1953).
[8]G. H. Newsom, Astrophys. J. 166, 243 (1971).
[9]R. Haensel, G. Kittel, B. Sonntag, C. Kunz, and P. Schreiber, Phys. Status Solidi A 2, 85 (1970).
[10]Y.-Y. Kim and P. S. Bagus, J. Phys. B 5, L193 (1972).
[11]P. L. Altick and A. E. Glassgold, Phys. Rev 133, 632 (1964).
[12]M. Ya Amusia, N. A. Cherepkov, I. Pavlin, V. Radojević, and Dj Zivanovic, J. Phys. B 10, 1413 (1977).
[13]M. Ya. Amusia and N. A. Cherepkov, Case Stud. At. Phys. 5, 47 (1975).
[14]C. M. Lee and W. R. Johnson, Phys. Rev. A 22, 979 (1980).
[15]J. W. Cooper and S. T. Manson, Phys. Rev. 177, 157 (1969).
[16]S. T. Manson, Chem. Phys. Lett. 19, 76 (1973).
[17]D. J. Kennedy and S. T. Manson, Phys. Rev. A 5, 227 (1972).
[18]S. T. Manson, Adv. Electron. Electron Phys. 41, 73 (1976).
[19]E. J. McGuire, Phys. Rev. 175, 20 (1968).
[20]J. Cooper and R. N. Zare, J. Chem. Phys. 48, 942 (1968).
[21]J. W. Cooper, Phys. Rev. 128, 681 (1962).
[22]J. W. Cooper, Phys. Rev. Lett. 13, 762 (1964).
[23]J. Berkowitz, *Photoabsorption, Photoionization and Photoelectron Spectroscopy* (Academic, New York, 1979).
[24]Y. S. Kim, A. Ron, R. H. Pratt, B. R. Tambe, and S. T. Manson, Phys. Rev. Lett. 46, 1326 (1981).
[25]C. E. Moore, *Atomic Energy Levels,* National Bureau of Standards (U.S.) Circ. No. 467 (U.S. GPO, Washington, D.C., 1971), Vol. I.
[26]S. T. Manson and J. W. Cooper, Phys. Rev. 165, 126 (1968).
[27]J. W. Cooper and R. N. Zare, Lect. Theor. Phys. 11C, 323 (1969).
[28]T. E. H. Walker and J. T. Waber, J. Phys. B 7, 674 (1974).
[29]U. Fano and J. W. Cooper, Rev. Mod. Phys. 40, 441 (1968).
[30]S. T. Manson, J. Electron Spectrosc. Relat. Phenom. 1, 413 (1973).
[31]S. T. Manson and A. F. Starace, Rev. Mod. Phys. 54, 389 (1982).
[32]N. A. Cherepkov, J. Phys. B 11, 1435 (1978).
[33]N. A. Cherepkov, J. Phys. B 12, 1279 (1979).
[34]K.-N. Huang, Phys. Rev. A 22, 223 (1980).
[35]K.-N. Huang, W. R. Johnson, and K. T. Cheng, Phys. Rev. Lett. 43, 1658 (1979).
[36]M. J. Seaton, Rev. Mod. Phys. 30, 979 (1958).
[37]M. J. Seaton, Proc. R. Soc. London 88, 801 (1966).
[38]U. Fano, Phys. Rev. 124, 1866 (1961).
[39]W. R. Johnson, K. T. Cheng, K.-N. Huang, and M. Le Dournef, Phys. Rev. A 22, 989 (1980).
[40]T. N. Chang and U. Fano, Phys. Rev. A 13, 263 (1976).
[41]B. Edlen, Handb. Phys. 27, 80 (1964).
[42]L. M. Biberman and G. E. Norman, Usp. Fiz. Nauk. 91, 193 (1967) [Sov. Phys.—Usp. 10, 52 (1967)].